AIP Journal of Applied Physics

Lithium implantation at low temperature in silicon for sharp buried amorphous layer formation and defect engineering

E. Oliviero, M. L. David, P. F. P. Fichtner, M. F. Beaufort, and J. F. Barbot

Citation: Journal of Applied Physics **113**, 083515 (2013); doi: 10.1063/1.4793507
View online: http://dx.doi.org/10.1063/1.4793507
View Table of Contents: http://scitation.aip.org/content/aip/journal/jap/113/8?ver=pdfcov
Published by the AIP Publishing

Lithium implantation at low temperature in silicon for sharp buried amorphous layer formation and defect engineering

E. Oliviero,[1,a)] M. L. David,[2] P. F. P. Fichtner,[3] M. F. Beaufort,[2] and J. F. Barbot[2]
[1]*CSNSM, CNRS-IN2P3-Université Paris-Sud, Bâtiment 108, 91405 Orsay, France*
[2]*Institut Pprime, CNRS-Université de Poitiers-ENSMA, SP2MI, Bd Marie et Pierre Curie, BP30179, 86962 Futuroscope-Chasseneuil Cedex, France*
[3]*Departamento de Metalurgia, Universidade Federal do Rio Grande do Sul, Av Bento Gonçalves 9500, Caixa Postal 15051, 90035-190 Porto Alegre, RS, Brazil*

(Received 17 January 2013; accepted 11 February 2013; published online 26 February 2013)

The crystalline-to-amorphous transformation induced by lithium ion implantation at low temperature has been investigated. The resulting damage structure and its thermal evolution have been studied by a combination of Rutherford backscattering spectroscopy channelling (RBS/C) and cross sectional transmission electron microscopy (XTEM). Lithium low-fluence implantation at liquid nitrogen temperature is shown to produce a three layers structure: an amorphous layer surrounded by two highly damaged layers. A thermal treatment at 400 °C leads to the formation of a sharp amorphous/crystalline interfacial transition and defect annihilation of the front heavily damaged layer. After 600 °C annealing, complete recrystallization takes place and no extended defects are left. Anomalous recrystallization rate is observed with different motion velocities of the a/c interfaces and is ascribed to lithium acting as a surfactant. Moreover, the sharp buried amorphous layer is shown to be an efficient sink for interstitials impeding interstitial supersaturation and {311} defect formation in case of subsequent neon implantation. This study shows that lithium implantation at liquid nitrogen temperature can be suitable to form a sharp buried amorphous layer with a well-defined crystalline front layer, thus having potential applications for defects engineering in the improvement of post-implantation layers quality and for shallow junction formation. © *2013 American Institute of Physics*.
[http://dx.doi.org/10.1063/1.4793507]

I. INTRODUCTION

Understanding and controlling the damage formation in silicon during ion implantation as well as damage recovery is crucial for the development of technologies that involve ion implantation.[1] Under specific conditions, implantation can lead to the transformation of the crystalline Si (*c*-Si) into the amorphous state (*a*-Si) when the free energy of the amorphous phase is lower than the highly damaged crystal. Indeed, amorphous Si has an enthalpy of ~0.13 eV/at higher than the undamaged *c*-Si.[2]

Nowadays, a renewed interest in amorphization/recrystallization has arisen due to several technological applications. For instance, amorphization/templated recrystallization can be used to change the orientation of single crystal silicon.[3] It is also widely used for the fabrication of nanometric-scale Si devices with the method of pre-amorphization and solid-phase epitaxial growth (SPEG) for ultra-low energy, high energy, or high fluence dopant implantation. In this method, pre-amorphization of single silicon crystal by ion-implantation efficiently eliminates the channelling of subsequent dopant implants, reduces the transient enhanced diffusion (TED) of dopants, and increases activation, thus resulting in shallow junction formation.[4–6] Generally, pre-amorphization is achieved by Si, Ge, or BF_2 implants. However, pre-amorphization implantation with such elements creates a damage band, rich in interstitials known as the end-of-range (EOR) defects beyond the amorphous/crystalline (a/c) interface. During the post-implantation activation annealing process, the EOR defects agglomerate into extended defects (dislocation loops and {311} defects), which can be responsible for junction leakage. The dissolution/evolution of these extended defects upon subsequent anneals injects interstitials towards both the surface and the bulk causing dopant diffusion and activation anomalies. Therefore, to improve defect engineering, it is important to be able to eliminate/control these extended defects.[7] Pre-amorphization with lighter elements than silicon could provide a solution. In this paper, the effect of lithium implantation is investigated. Lithium is also an interesting element to be inserted into silicon, as silicon is a candidate for new generation of Li-batteries[8] and it is important to understand properties of silicon in lithiated state.[9]

The aim of this paper is twofold. First, it is shown that the use of lithium ion implantation at low temperature produces a sharp buried amorphous layer close to the surface. Special emphasis is given on the a/c interface and on the remaining defects after recrystallization. Second, it is shown that the buried amorphous layer created by lithium implantation impedes the formation of interstitial-related extended defects in case of noble gas subsequent implantation, suggesting application of such layers for defect engineering. For that purpose, neon implantation was deliberately chosen

[a)]Research performed while E. Oliviero was at Instituto de Fisica, Universidade Federal do Rio Grande do Sul, Porto Alegre, Brazil.

because it was shown to produce a high density of elongated interstitial defect.[10]

II. EXPERIMENTAL CONDITIONS

All the experiments were performed on commercial Czochralski-grown n-type (100) silicon wafers. The resistivity of the wafers was 1–2 Ω cm. Samples were implanted at a fluence of 7×10^{15} ions cm^{-2} with 150 keV lithium ions. The beam flux was 5×10^{12} ions cm^{-2} s^{-1}. Implantations were carried out at liquid nitrogen temperature to favor target amorphization. Anneals were performed in a vacuum of $\sim 10^{-7}$ Torr at temperatures ranging from 100 to 800 °C for 30 min in a quartz tube within a tubular furnace. As-implanted and annealed samples were investigated by Rutherford backscattering spectrometry under channeling conditions (RBS/C) using an incident beam of 1.6 MeV $^4He^+$ from a 3 MV Tandetron in random or in ⟨100⟩ crystal directions. The damage depth profiles were determined from the RBS spectra using the surface energy approximation outlined in Ref. 11.

Neon implantation was carried out at 50 keV to a fluence of 2×10^{16} Ne^+ cm^{-2} at a flux of 6×10^{12} ions cm^{-2} s^{-1}. The implantation energy was chosen so that the neon's distribution is located in the front layer, away from the buried amorphous layer created by the lithium implantation. Stopping and Range of Ions in Matter (SRIM) calculations[12] give a mean projected range (R_p) of 110 nm and an ion straggling (ΔR_p) of 43 nm. In that case, implantations were carried out at 250 °C to avoid further amorphization.

Annealing at 800 °C for 30 min was proceeded in a quartz tube within a tubular furnace under a vacuum of $\sim 10^{-7}$ Torr and with argon flux.

All the samples, at the different stages of processing, were prepared in cross-section geometry for TEM investigations. XTEM samples were cut, glued, and then thinned using tripod mechanical polishing to about 7 μm thick and then argon milling up to electron transparency. Thin cross sections were then studied using a JEOL 2010 and a FEI Tecnai G2 20. In order to avoid defect creation due to electron irradiation, an accelerating voltage of 150 kV (below the threshold voltage for point defects formation of 170 kV) was chosen unless otherwise mentioned. To study cavities created by the neon implantation with minimal contrast from the unavoidable accompanying lattice damage, specimens were tilted from their ⟨100⟩ orientation by few degrees in order to reduce diffraction effects. They were also imaged in under-focus and over-focus conditions to highlight the cavity edges with Fresnel contrast. In the following, S in the TEM images denotes the implanted surface of the sample

III. RESULTS AND DISCUSSION

A. Buried amorphous layer

Lithium implantation at liquid nitrogen temperature creates a buried amorphous layer starting approximately 400 nm below the surface and extending to a depth of 960 nm as shown in the XTEM image in Figure 1(a). Actually, a three layers structure is observed: a buried amorphous layer surrounded by two

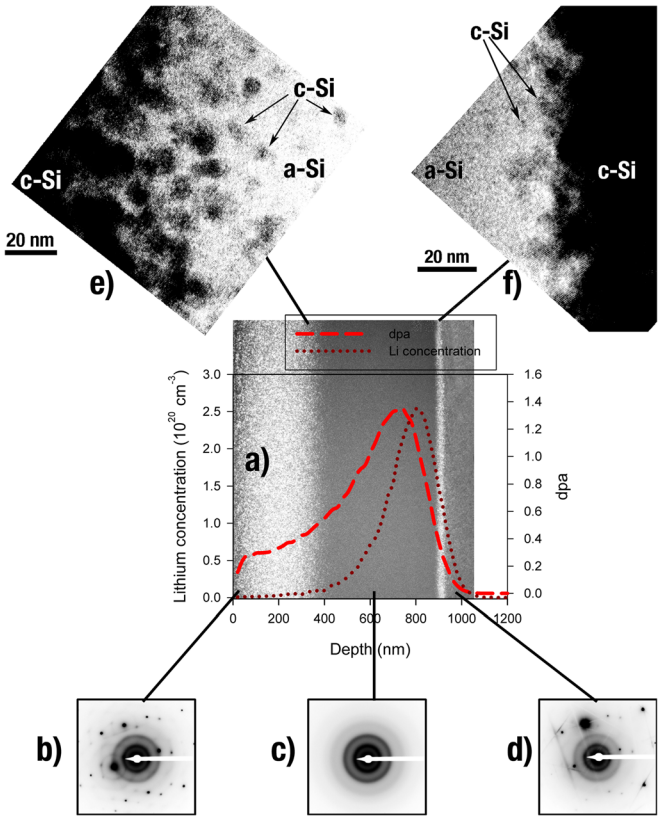

FIG. 1. XTEM images of Si implanted with Li (150 keV and 7×10^{15} cm^{-2}) at liquid nitrogen temperature: (a) WBDF taken at g_{111} of as-implanted sample and superimposed SRIM calculation, (b) selected area diffraction pattern of the front region, (c) selected area diffraction pattern of the buried layer, (d) selected area diffraction pattern of the rear region, (e) HRTEM of front a/c interface taken on (101) axis, (f) HRTEM of upper a/c interface taken on (101) axis.

highly damaged crystalline layers. Both the upper and lower amorphous-crystalline interfaces are rough.

A high resolution TEM (HRTEM) analysis shows that the two surrounding layers are not completely crystalline (Figures 1(e) and 1(f)). The front layer, 400 nm wide, is composed of a mixture of crystalline and amorphous zones. In the selected area diffraction (Figure 1(b)), a diffracted spot pattern is overlapping a Debye-Scherrer ring pattern, indicating a wide and gradual transition before a continuous amorphous layer (Figure 1(c)). The back layer has the same aspect but is much thinner, approximately 50 nm (Figure 1(d)). This state, including the two phases and that can be described as a mixed-phase region, corresponds to displacements between 0.1 dpa and 0.5 dpa (calculated with SRIM simulations[12] with a displacement energy of 15 eV and a binding energy of 2 eV). Calculations of the Boltzmann transport equation together with RBS/C measurements have shown that 10% of displacement was enough to start amorphizing Si at 77 K,[13] i.e., 0.1 dpa. It should be noted that for such dpa values, only amorphous pockets are formed as observed in TEM (Figure 1(b)) and full amorphization is not yet reached even if in RBS/C the yield is equal to that of random spectra indicating a highly disordered region (see Figure 3). Great care should be taken in analyzing RBS/C spectra in the as-implanted state to define the amorphous region.

For dpa values higher than 0.5 (0.5 dpa $= 5 \times 10^{22}$ eV/cm^3 $= 1$ eV/at), full amorphization is reached (Figure 1(c)). Implanting at LN_2 temperature is an ideal case to use the dpa threshold model for amorphization (i.e., homogeneous amorphization) since all recombination, defect annihilation, or diffusion are restricted. Evidently, for room temperature implantation, significantly higher value for the amorphisation threshold is found due to dynamic defect annihilation and depends on various implantation parameters (flux and ion mass for example). Priolo and Rimini[14] give a threshold value of ~13 eV/at and Pelaz *et al.*[15] report a value of 5×10^{23} eV/cm^3 (10 eV/at).

Annealing at 400 °C-30 min clearly does not induce SPEG recrystallization of the buried layer but removes front and rear defects in the mixed-phase regions, leaving sharper a/c interfaces and a good crystalline layer in front (see Figure 2(b)). It should be noted that the rear a/c interface is much better defined than the front one. From the strong black contrast on the TEM images, it can be assumed that the crystalline front layer is strained. The recrystallization of the front layer at such low temperature could be explained by a stress-enhanced recrystallization as already proposed by Holland *et al.*[16] Although, recent results obtained by Rudawski *et al.*[17] show that uniaxial stress has no effect on SPEG velocity of the planar interfaces for in-plane tension

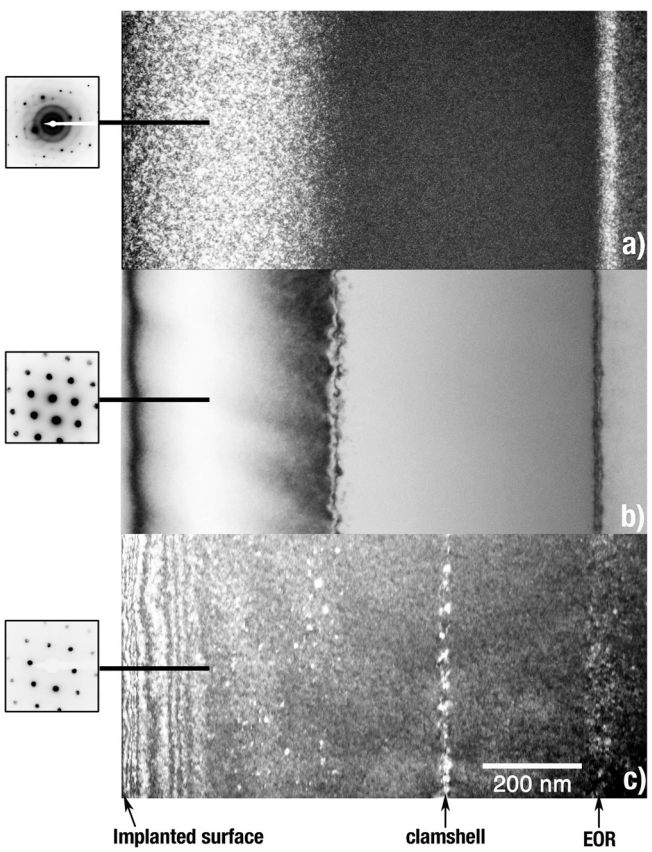

FIG. 2. XTEM images of Si implanted with Li (150 keV and 7×10^{15} cm^{-2}) at nitrogen temperature: (a) WBDF taken at g_{111} of as-implanted, (b) bright field after annealing at 400 °C-30 min, (c) WBDF taken at g_{111} after annealing at 600 °C-30 min. The vertical contrast close to the surface is an artifact produced during specimen preparation. In the insets, selected area diffraction pattern from the area indicated by the arrow.

though compression does cause significant retardation. But in our case, recrystallization does not concern planar interfaces but more spherical amorphous zones. Thus, in the mixed-phase region, recrystallization can take place at low temperature certainly due to an effect of the stress.

After 600 °C annealing, Figure 2(c), complete recrystallization of the buried layer is observed. Residual defects identified as clamshell defects are observed in the "ex-amorphous zone." Their formation is attributed to closure problems at the intersection of the two SPEG regrowth fronts.[18] Defects are also present at the original a/c interface positions and at the back of the "ex-amorphous zone" in the region of EOR (see arrow in Figure 2(c)). However, their density is low and in RBS spectra the maximum yield is near 0% (Figure 3). It should be noted that no threading dislocations or regrowth-related defects are observed comparing to Si self-ion implantation[14,19] or like recently observed in Ge when amorphized by Si ions where after 650 °C anneal a high density of threading dislocations is still present.[20] Moreover, at the anneal temperatures used, no {311} defects are formed. In self-implanted Si at RT or at 77 K, {311} defects are already formed after annealing at the end of range region.[16,19,21,22] This points out the peculiarity of Li implantation at low temperature.

Figure 3 shows the annealing behavior of the Li implantation induced damage after annealing at different temperatures, studied by RBS. At 100 °C, part of the defects present between the surface and the amorphous layer is first annealed. The near surface region stays highly disturbed and the EOR region unchanged. For 200 °C anneal, a significant reduction of the yield is observed over the first 250 nm. In this region, the yield is at the same level to that of the unimplanted sample. All defects from the surface have also disappeared, while in the EOR region no significant changes are observed. 300 °C anneal has no further effect but 400 °C anneal leads to a sharper front a/c interface. The region free of defects now extends up to 300 nm. In the EOR region, no significant changes are observed even if by TEM the a/c interface is seen to become sharper (Figure 2(b)). At 500 °C, asymmetrical recrystallization takes place resulting in the shrinking of the amorphous layer of ~70 nm in front and ~20 nm in the back. Complete recrystallization of the amorphous layer occurs at 600 °C and no residual defect is detected by RBS.

Considering the speed of SPEG recrystallization (Eq. (1)) given by Olson and Roth[23] for an a-Si layer on top of (100) oriented c-Si, the width of the layer that should recrystallize during the annealing at 500 °C can be estimated. The SPEG velocity is given by

$$v_R(\text{nm/s}) = v_0 \exp\left(\frac{-E_a}{kT}\right), \tag{1}$$

where E_a is the activation energy for recrystallization ($E_a = 2.68$ eV), v_0 is the initial velocity ($v_0 = 3.08 \times 10^{15}$ nm s^{-1}), k the Boltzmann constant, and T the temperature of annealing.

Applying this equation with our annealing conditions, no significant SPEG recrystallization should occur for 400 °C anneal (0.047 nm), while for 500 °C anneal a layer of

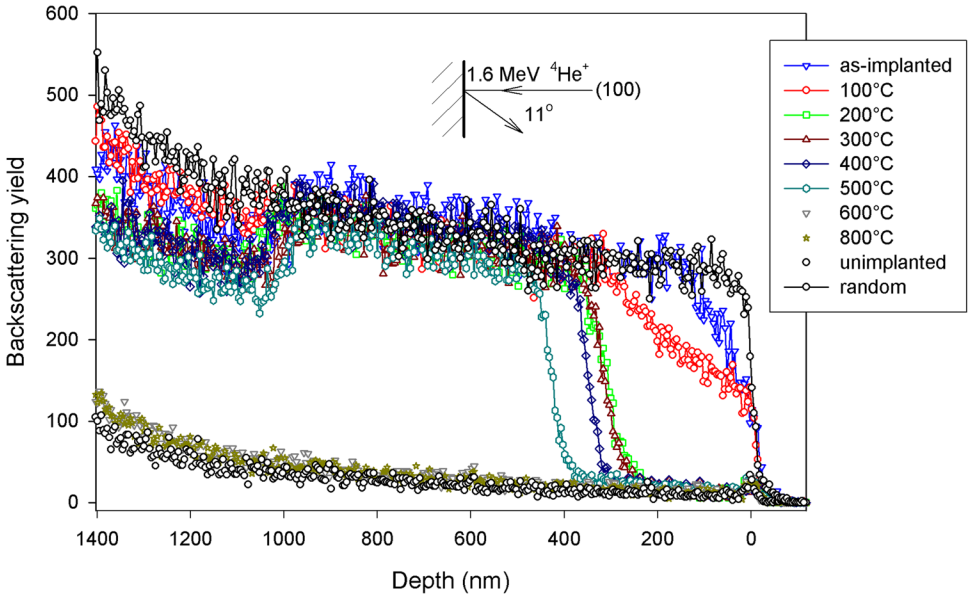

FIG. 3. Evolution of the RBS/C spectra obtained after Li implantation (150 keV and 7×10^{15} cm^{-2}) at liquid nitrogen temperature for increasing isochronal (30 min) annealing temperature.

19 nm should recrystallize. In our RBS study, we found that approximately 70 nm ± 5 nm has recrystallized from the front a/c interface and 20 nm ± 5 nm from the back a/c interface (Figure 4(b)). The recrystallization of the front a/c interface has thus been enhanced. This enhancement could be explained by the presence of Li and/or the presence of defects at the vicinity of the a/c interface.

Impurities are able to enhance or retard the motion velocity of the a/c interface during recrystallization.[24] However, it should be noted that the as-implanted Li distribution is asymmetric in the regions adjacent to the a/c interfaces (Figure 4(a)) and should not have much influence on the front a/c interface. Even if little is known on Li behavior in Si, it can be underlined that inserted Li atom in c-Si energetically prefers a tetrahedral interstitial site while exhibiting a shallow donor level and has a high mobility in c-Si with a diffusion barrier of 0.6 eV.[25] The interaction Li-Li between Li impurities is repulsive, indicating a rather low probability for Li agglomeration.[26] However, Si_xLi_y alloys can be formed if a high dose of Li is inserted. Lithiation will then rather easily lead to destabilization of the host Si network (i.e., amorphization) and subsequent formation of new Si_xLi_y alloy phases, accompanied with significant volume expansion.[25] Crystalline silicon amorphizes at a ratio of 0.3 Li atoms per Si atom,[26] which means for a local Li concentration of 1.5×10^{22} at/cm^3, i.e., far from our implanted maximum of 2.5×10^{20} Li/cm^3. Thus, in the first step of recrystallization, Li atoms must stay in interstitial position and should not play a significant role.

Amorphous silicon obtained by ion implantation is less dense than crystalline silicon. Recrystallization is the process to get back to the same density, i.e., a flux of interstitials is needed. A flux of Si interstitials atoms to the a/c interface can thus enhance recrystallization. As observed in Figure 1, a large amount of defects are present in the front of the front a/c interface. These defects disappear during annealing (Figure 2(b)). Thus, during the first step of annealing, it can act as a source of interstitials for recrystallization, leading to an enhancement of the process. Moreover, as explained above, the mixed-phase region close to the front interface can start to recrystallize at lower temperature (see Figure 3, 200 °C annealing).

It should be noted that this enhancement decreases as recrystallization takes place (certainly as the interstitial source dries up). After complete recrystallization (Figure 4(c)), the meeting of the two interfaces is not observed in the middle of the previous amorphous layer but closer to the implanted surface. Two different scenarios can then be considered: (i) the front recrystallization front is now delayed, while the back front velocity stays normal, i.e., the front recrystallization changes from enhancement to retardment. (ii) The front recrystallization front velocity becomes normal, while the back front velocity is now enhanced, i.e., a faster recrystallization from the back interface. So, in a second step, retardation of the front interface and/or a SPEG enhancement of the back interface might occur. This inversion takes place when the a/c interfaces approach the center of the amorphous zone: the defects-mediated recrystallization is overcome by Li-mediated recrystallization.

As observed for Fe,[24] Ne,[10] or He,[27] Li atoms present in the amorphous layer must be swept by the recrystallization front. This leads to a high concentration of Li in the middle. When the back interface meets the maximum concentration (Figure 4(b)), Li can act as a surfactant, i.e., inducing an enhancement of recrystallization (equivalent to the use of species to improve crystal growth[28]). Recently, the use of additional surface species (surfactants) that can modify the epitaxial growth has attracted a lot of interest. In surfactant-mediated epitaxy, a monolayer of surfactant material floats at the growth front and influences the epitaxial growth.

Further investigations are needed to clearly understand this phenomenon by following recrystallization by *in situ* TEM experiments.

B. Sink for interstitials

In the case of neon implantation, it has been shown that the formation of cavities is accompanied by the formation of

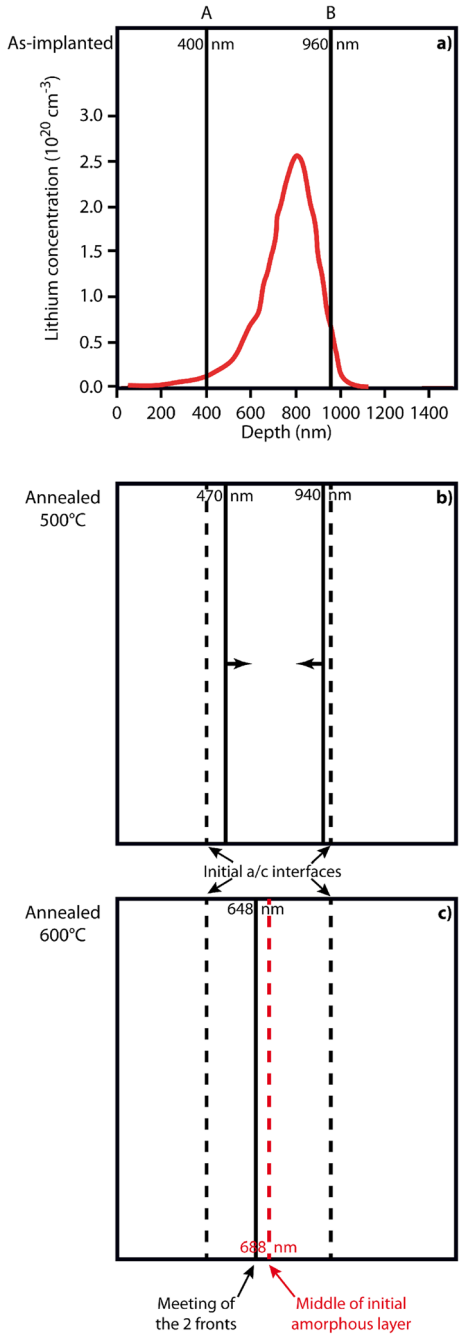

FIG. 4. Schematic evolution of the amorphous layer obtained after Li implantation (150 keV and 7×10^{15} cm^{-2}) at nitrogen temperature with annealing temperature (30 min).

extended defects.[10] Figure 5 shows a cross-sectional TEM image of silicon sample obtained after implantation with neon at 50 keV, 250 °C followed by annealing at 800 °C for 30 min. Bubbles are forming a 250 nm wide layer starting at the implanted surface. Two different regions can be distinguished. From the surface up to 50 nm, small bubbles of about ~2 nm in diameter are observed. Then, from 50 up to 250 nm larger bubbles are formed. Their mean diameter is about 14 nm (±2 nm).

The 50 nm wide tiny bubble band corresponds to a zone that was free of interstitial clusters in the as-implanted sample. During implantation, the surface acts as a sink for interstitials that are mobile at the temperature used. The same

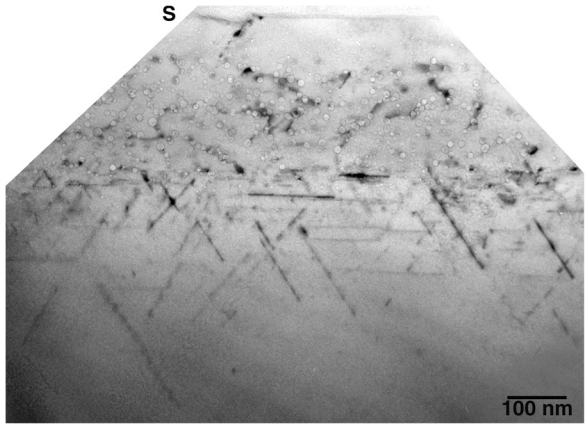

FIG. 5. Cross-sectional TEM micrograph of silicon sample implanted at 250 °C with 50 keV Ne at a fluence of 2×10^{16} cm^{-2} after annealing at 800 °C for 30 min. Underfocus image acquired in kinematical diffraction conditions.

phenomenon occurs with vacancies during growth of bubbles, i.e., during annealing. A limited Ostwald ripening can explain the formation of tiny bubbles in the 50 nm front region: the proximity of the surface inhibits the growth of bubbles since it is acting as a sink for vacancies. No faceting of the bubbles is observed. A high density of elongated defects is observed beyond the bubble layer, at the ions end-of-range, between 260 nm and 730 nm from the surface. These almost one-dimensional faulted defects extended over large distance towards the bulk along specific ⟨110⟩ directions. They lie on {311} planes and have lengths ranging from 30 to 200 nm. They have been therefore identified as {311} or "rod-like" defects with a Burgers vector of a/25⟨116⟩. These defects result from the agglomeration of supersaturated Si self-interstitials.[29] The formation of such extended structures is still not very well understood. Obviously, that begins with individual interstitials which trap each other and form I_2 and I_3, up to large I_n clusters. In the condition of supersaturation, self-interstitials in silicon have the tendency to cluster. The driving force for such a precipitation process is the reduction of the chemical potential for an interstitial Si atom forming such a defect (a single interstitial being less stable than a cluster). {311} defects thus consist of a stacking of I_2 or I_3 (in the form of (110) chains of Si self-interstitials) stored in a stable configuration.[30] Twelve variants of this type of defects exist (elongated along the six ⟨110⟩ directions with two possible habit planes for each direction). Four variants are lying parallel to the {100} implanted surface.[29,30] Some dislocation networks are observed within the bubble layer.

The sharp buried layer formed by Li implantation described in Sec. III A was used to study how interstitials, produced by neon implantation, interact with such structure. It is imperative to have a buried amorphous layer with a good crystalline zone in front because if gas is implanted directly inside the amorphous zone, post-annealing treatment leads to the formation of microtwin, defects, and polycrystals.[10,27] Neon was thus implanted in the front crystalline and free of defects region of the Li implanted sample. After neon implantation in the front layer, small bubbles are formed (Figure 6(a)). No much difference is observed

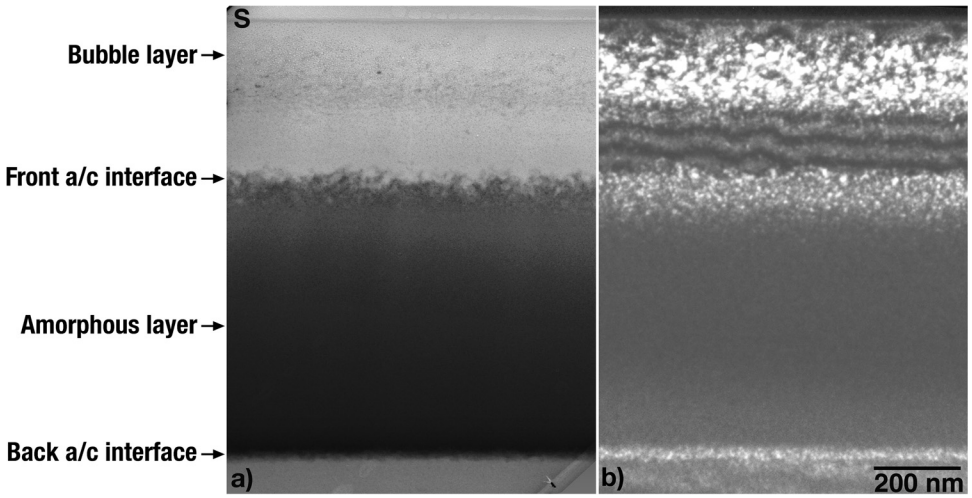

FIG. 6. Cross-sectional TEM micrographs of silicon sample implanted at 77 K with 150 keV Li at a fluence of 7×10^{15} cm^{-2}, annealed at 400 °C for 30 min and subsequently implanted at 250 °C with 50 keV Ne at a fluence of 2×10^{16} cm^{-2}: (a) Bright field image. (b) WBDF image (g, 5g) g = ⟨111⟩.

compared to the case where neon is implanted in virgin silicon.[31] Dark contrast is also observed in the bright field image of Figure 6(a), while defects are clearly observed in the bubble band region in the weak beam dark field (WBDF) image of Figure 6(b). Moreover, the front a/c interface has suffered from the second implantation and is not sharp anymore (see arrow in Figure 6(b)). Damage is accumulated at both a/c interfaces and more significantly at the front one as compared to Figure 2(b).

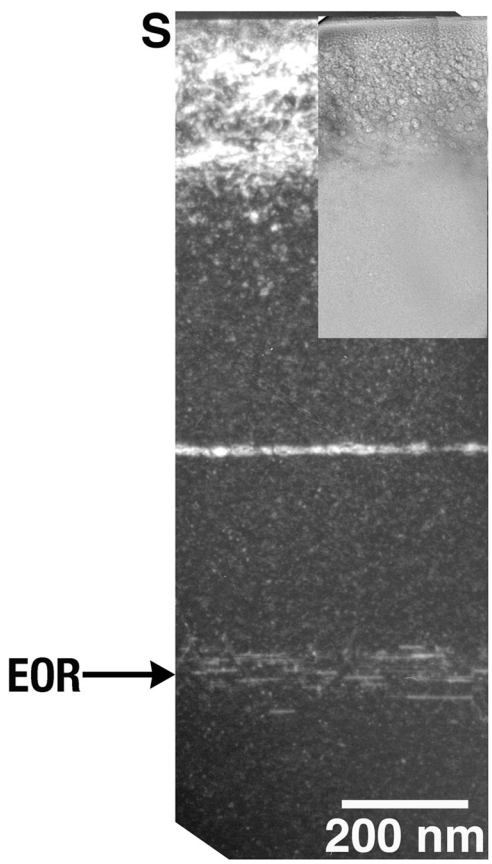

FIG. 7. Cross-sectional TEM (accelerating voltage 200 kV) micrographs of silicon sample implanted at 77 K with 150 keV Li at a fluence of 7×10^{15} cm^{-2}, annealed at 400 °C for 30 min and subsequently implanted at 250 °C with 50 keV Ne at a fluence of 2×10^{16} cm^{-2} and annealed at 800 °C for 30 min: WBDF image (g, 5g) g = ⟨100⟩. In the inset, bright field image of the bubble layer.

After annealing at 800 °C for 30 min of the co-implanted Li-Ne system, the complete recrystallization of the buried amorphous layer occurs as expected from the SPEG model, see Figure 7. At the same time, bubbles grow and form a dense and uniform layer (see Figure 7(a)). The striking effect is that contrary to what was observed after annealing of neon implanted virgin silicon (Figure 5), no extended defects are formed close to the bubble layer. Only residual defects from the ex front a/c interface are observed in the WBDF image in Figure 7(b). Clamshell defects are again observed at the meeting point of the two moving interfaces in the ex amorphous layer. Extended defects are also present at the original back a/c interface position in the region of EOR. They are elongated along ⟨110⟩ directions and lie in {311} planes and were therefore identified as {311} defects. The formation of these defects at the EOR in case of dual implantation results from the neon implantation, which adds extra interstitial defects. Moreover, neon implantation was carried out at 250 °C so that interstitials are highly mobile in silicon and certainly are also mobile in a-Si. Self-interstitial diffusion through Si amorphous layer might occur and leads to supersaturation in this region.

It seems that the buried amorphous layer acts as an effective sink for interstitials. As previously seen, the a/c interface can trap some interstitials. Moreover, the difference in density between amorphous and crystalline silicon makes the amorphous layer demanding in interstitials.

Another effect of the interaction with the buried layer is that the size of the neon bubbles is slightly higher and the density is significantly higher than for the single implantation. This can be explained again by the trapping of interstitials at the buried amorphous layer, lowering the flux of interstitials toward the surface, and therefore limiting the interaction of interstitials with cavities. Cavities are indeed traps for interstitial. They can shrink or even disappear if a high quantity of interstitials is provided.[32] Interstitials do not play any role in the cavities growth, which certainly occurs by migration and coalescence of already formed small bubbles. However, when not trapped, they can interact with the cavities after the growth, inducing a general shrinkage and the dissolution of some cavities.

IV. CONCLUSION

In summary, lithium implantation at liquid nitrogen temperature in silicon followed by a low temperature annealing leads to the formation of sharp buried amorphous layer with a front layer free of defects. After recrystallization, a very low concentration of residual defects is found at the end of range of lithium ion. In contrast to what was observed by Clark *et al.*,[33] who showed that increase of the ion mass decreases the population of interstitial trapped in the EOR, this study shows that for low temperature implantation, low ion mass induces less defects.

Moreover, it was shown that buried amorphous layer acts as an efficient sinks for interstitial. A high density of {311} defects located close to a neon bubbles layer was successfully suppress. This type of structure can be used in the development of defects engineering in silicon and other materials.

ACKNOWLEDGMENTS

The authors would like to thank A. Bula and C. Castello for the implantations and L. Pizzagalli for fruitful discussion and for critical reading of the paper. E. Oliviero would like to acknowledge the CNPq for funding (Processo No. 150368/2003-8) and the authors acknowledge CAPES-COFECUB funding.

[1]ITRS 2007 Front End Process Update.
[2]S. Roorda and W. C. Sinke, Phys. Rev. B **44**, 3702 (1991).
[3]K. L. Saenger, J. P. de Souza, K. E. Fogel, J. A. Ott, A. Reznicek, C. Y. Sung, and D. K. Sadana, Appl. Phys. Lett. **87**, 221911 (2005).
[4]M. Delfino, D. K. Sadana, and A. E. Morgan, Appl. Phys. Lett. **49**, 575 (1986).
[5]E. Napolitani, A. Coati, D. De Savador, A. Carnera, S. Mirabella, S. Scalese, and F. Priolo, Appl. Phys. Lett. **79**, 4145 (2001).
[6]M. Xu, G. Regula, R. Daineche, E. Oliviero, B. Hakim, E. Ntsoenzok, and B. Pichaud, Thin Solid Films **518**, 2354 (2010).
[7]E. Oliviero, M. L. David, and P. F. P. Fichtner, Phys. Status Solidi C **6**, 1969 (2009).
[8]C. K. Chan *et al.*, Nat. Nanotechnol. **3**, 31 (2008).
[9]A. Kushima, J. Y. Huang, and J. Li, ACS Nano **6**, 9425 (2012).
[10]E. Oliviero, S. Peripolli, L. Amaral, P. F. P. Fichtner, M. F. Beaufort, J. F. Barbot, and S. E. Donnelly, J. Appl. Phys. **100**, 043505 (2006).
[11]W. K. Chu, J. W. Mayer, and M. A. Nicolet, *Backscattering Spectrometry* (Academic, New York, 1978).
[12]J. F. Ziegler, J. P. Biersack, and U. Littmark, *The Stopping and Range of Ions in Solids* (Pergamon, New York, 1985).
[13]L. A. Christel, J. F. Gibbons, and T. W. Sigmon, J. Appl. Phys. **52**, 7143 (1981).
[14]F. Priolo and E. Rimini, Mater. Sci. Rep. **5**, 319 (1990).
[15]L. Pelaz, L. A. Marqués, and J. Barbolla, J. Appl. Phys. **96**, 5947 (2004).
[16]O. W. Holland, C. W. White, M. K. El-Ghor, and J. D. Budai, J. Appl. Phys. **68**, 2081 (1990).
[17]N. G. Rudawski, K. S. Jones, and R. Gwilliam, Appl. Phys. Lett. **91**, 172103 (2007).
[18]K. S. Jones, S. Prussin, and E. R. Weber, Appl. Phys. A **45**, 1 (1988).
[19]M. K. El-Ghor, O. W. Holland, C. W. White, and S. J. Pennycook, J. Mater. Res. **5**, 352 (1990).
[20]D. P. Hickey, Z. L. Bryan, K. S. Jones, R. G. Elliman, and E. E. Haller, Appl. Phys. Lett. **90**, 132114 (2007).
[21]O. W. Holland and C. W. White, Nucl. Instrum. Methods Phys. Res. B **59–60**, 353 (1991).
[22]J. Li and K. S. Jones, Appl. Phys. Lett. **73**, 3748 (1998).
[23]G. L. Olson and J. A. Roth, Mater. Sci. Rep. **3**, 1 (1988).
[24]J. P. de Souza, L. Amaral, and P. F. P. Fichtner, J. Appl. Phys. **71**, 5423 (1992).
[25]H. Kim, K. E. Kweon, C.-Y. Chou, J. G. Ekerdt, and G. S. Hwang, J. Phys. Chem. C **114**, 17942 (2010).
[26]S. C. Jung and Y.-K. Han, Electrochim. Acta **62**, 73 (2012).
[27]M. F. Beaufort, L. Pizzagalli, A. S. Gandy, E. Oliviero, D. Eydi, and S. E. Donnelly, J. Appl. Phys. **104**, 094905 (2008).
[28]M. Copel, M. C. Reuter, E. Kaxiras, and R. M. Tromp, Phys. Rev. Lett. **63**, 632 (1989).
[29]I. G. Salisbury and M. H. Loretto, Philos. Mag. A **39**, 317 (1979).
[30]S. Takeda, M. Kohyama, and K. Ibe, Philos. Mag. A **70**, 287 (1994).
[31]E. Oliviero, S. Peripolli, P. F. P. Fichtner, and L. Amaral, Mater. Sci. Eng., B **112**, 111 (2004).
[32]A. V. Fedorov, A. van Veen, H. Schut, and A. Rivera, Nucl. Instrum. Methods Phys. Res. B **148**, 289 (1999).
[33]M. H. Clark, K. S. Jones, T. E. Haynes, C. J. Barbour, K. G. Minor, and E. Andideh, Appl. Phys. Lett. **80**, 4163 (2002).